# Performance of diamond-like carbon-protected rubber under cyclic friction

Martinez-Martinez, D.; van der Pal, J. P. ; Pei, Y. T.; de Hosson, J. Th. M.

*Published in:*
Journal of Applied Physics

*DOI:*
10.1063/1.3665443



*Publication date:*
2011

# Performance of diamond-like carbon-protected rubber under cyclic friction. I. Influence of substrate viscoelasticity on the depth evolution

D. Martinez-Martinez,[a] J. P. van der Pal, Y. T. Pei, and J. Th. M. De Hosson
*Materials innovation institute M2i, Department of Applied Physics, University of Groningen, Nijenborgh 4, 9747 AG Groningen, Netherlands*

(Received 29 June 2011; accepted 29 October 2011; published online 20 December 2011)

In this paper, the influence of the viscoelastic properties of rubber substrate on the tribological behavior of DLC film-coated alkyl acrylate rubber is studied. The mechanical behavior of the rubber was first characterized by creep experiments using spherical indentations. The results were adjusted using a delayed elasticity model, and a numerical simulation of the indentation of the sliding counterpart ball during the tribotest was carried out. The results show a progressive increase of the contact depth, which is in agreement with the experimental observations. © *2011 American Institute of Physics*. [doi:10.1063/1.3665443]

## I. INTRODUCTION

In previous papers,[1–5] we have investigated the application of diamond-like carbon (DLC) films as an optimal protective coating for rubbers used as seals in ball bearings. DLC films were selected because of their excellent properties, like relatively high hardness, chemical inertness, low coefficient of friction (CoF), and low wear rate.[6] Their chemical composition based on C and H provided good compatibility and adhesion with the rubber-substrate materials.[1] The microstructure and flexibility of DLC films deposited with plasma-assisted chemical vapor deposition (PACVD) was tailored by tuning the growth conditions in terms of bias voltage and treatment time.[2,3] As a result, the temperature variation during film growth could be controlled,[2] which defined the thermal stresses in the system and thus the density of crack network. In addition, it was demonstrated that bias voltage did not produce a major influence on the chemical bonding in the DLC films,[3] and the differences in tribological performance among the films were mainly related to the different microstructures.[2]

The tribological performance of the DLC-protected rubbers is excellent, with negligible wear and much lower CoFs than the unprotected rubber.[1,2] For instance, Fig. 1 shows the reduction of CoF from 1.3–1.4 for unprotected alkyl acrylate (ACM) rubber to values below 0.25 after protection with a DLC film. The significant improvement in tribological performance can be attributed to the reduced adhesive interaction between the steel counterpart and the DLC film. The evolution of the CoF during the tribotest was demonstrated to depend on the viscoelastic properties of the rubber.[1] In fact, a parallel behavior of the ball depth and the CoF was observed (see also Fig. 1). However, the reasons for this kind of behavior are not clear.

The aim of this work is to evaluate the mechanical properties of the rubber substrate using the same contact geometry as used in the experiments, and to study their influence on the depth evolution of a wear track during the tribotest by a simple model. The frictional behavior requires a more complex approach, and it is described in another paper.[7]

## II. EXPERIMENTAL DETAILS

DLC thin films were deposited on alkyl acrylate (ACM) rubber by means of plasma-assisted chemical vapor deposition (PACVD) in a Teer UDP/400 close-field unbalanced magnetron sputtering rig, with all the magnetrons powered off. A pulsed dc (p-dc) power unit (Advanced Energy) was used as substrate bias source, operating at 250 kHz with a pulse-off time of 500 ns and voltages between 300 and 600 V. Before deposition, the rubber substrates were cleaned by two subsequent wash procedures using a detergent solution and boiling water, to improve the film adhesion by removal of the dirt and the wax present in the rubber, respectively.[2,8] The deposition process was composed by two etching steps in Ar and $Ar/H_2$ mixtures, respectively, followed by the deposition in an $Ar/C_2H_2$ environment. During these steps, the temperature of the rubber varied as a result of ions impingement, and the film microstructure could be tailored because of the different thermal stresses during the growth.[2] Further details about the deposition conditions can be found elsewhere.[1–3]

The tribological performance was evaluated at room temperature on a CSM tribometer with a ball-on-disk configuration, operating at $35 \pm 2\%$ relative humidity controlled by a humidity regulator. The counterpart was a ∅6-mm commercial 100Cr6 steel ball. The tribotest conditions were 1-N normal load, 20-cm/s sliding speed, and 10,000 laps length on a ∅18-mm wear track.

The estimation of the mechanical properties of rubber was done by creep experiments using a spherical indenter. The equipment used was a CSM Revetest scratch tester, setting the linear speeds to zero (i.e., indentation configuration) and using a ∅6-mm spherical tip. This arrangement is very adequate to mimic the conditions during a tribotest, because the loads and the indenter geometry are the same. The main difference is the much lower frequency when compared to the tribotest. Because the equipment used for performing the indentation does not allow working at constant load, the

[a]Author to whom correspondence should be addressed. Electronic mail: d.martinez-martinez@m2i.nl.

 

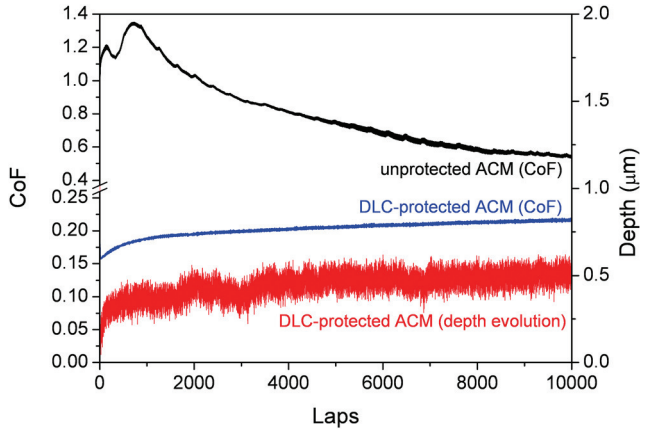


FIG. 1. (Color online) Tribological performance of uncoated and DLC film-coated ACM rubber.

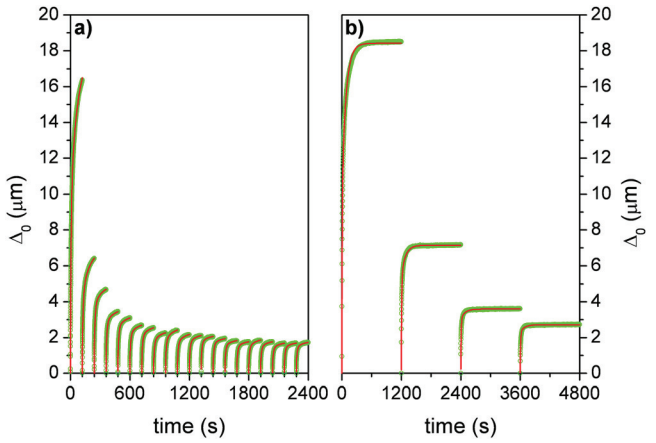


FIG. 2. (Color online) Creep measurement during spherical indentation on ACM rubber at 2 N load: (a) short indentations, and (b) long indentations. The points and lines represent the experimental data and fitting with Eq. (7), respectively.

minimum unloading rate (0.01 N/min) was used, which can be considered as a quasi-constant load-indentation process. The total indentation time for each indentation depends on the load limits. Two types of experiment were done for each load (1, 2, and 5 N), varying the number and duration of the indentations (Table I summarizes the conditions of the measurements performed at 2 N). In all cases, the initial load has been selected higher than the ending one to avoid possible effects of extra loading. Thus, at very long loading times (i.e., when a steady-state deformation is reached), small positive deformations (i.e., rubber recovery) might be expected (the load slightly decreases during the indentation), but they were not observed experimentally.

## III. RESULTS AND DISCUSSION

### A. Evaluation of mechanical properties of rubber

Figure 2 shows the results of both sets of creep experiments performed on ACM rubber. It can be seen that the deformation (indentation depth) $\Delta_0$ decreases with the number of cycles as the accumulated residual deformation from previous indentations becomes larger and larger. In addition, the depth during each cycle of the short creep indentations did not reach a steady state that was always observed during the long ones. Many different models can be considered to fit the viscoelastic behavior of materials. In particular, different arrangements of springs and dashpots have been typically used. A spring represents a perfect elastic behavior, and it is characterized by its resistance to deformation $g$, whereas a dashpot represents a perfect viscous deformation, and it is characterized by its viscosity $\eta$. The so-called Maxwell and Voigt models are the simplest possible arrangements of both elements, in series and in parallel, respectively (see Figs. 3(a) and 3(b)). The former one describes steady creep, whereas the latter one defines a purely viscoelastic deformation whose relaxation time ($T$) can be defined as:

$$T = \frac{\eta}{g}. \tag{1}$$

However, a Voigt model does not account for purely (immediate) elastic deformations, and typically a second spring is located in series with the Voigt unit, which also avoids an initial infinite force in relaxation tests.[9] This arrangement (Fig. 3(c)) is called a standard linear model (SLS), and therefore includes both elastic and viscoelastic deformations (a Maxwell unit in parallel with a spring is equivalent).

When a sphere of radius $R$ contacts under a normal force $F_0$, an elastic incompressible planar solid with shear modulus $G$, the radius and depth of contact ($a$ and $\Delta_0$, see Fig. 4) can be calculated by the Hertzian equation:[10]

$$a^3 = (R\Delta_0)^{3/2} = \frac{3}{8}\left(\frac{1}{2G}\right)RF_0. \tag{2}$$

According to Radok,[10,11] the solution for viscoelastic systems can be obtained by replacing the elastic constant in the elastic solution by the corresponding integral operator for the viscoelastic stress–strain relation. Because, in this particular case, the load history of the sample is known, the variation in deformation can be found from the elastic solution by

TABLE I. Experimental parameters of creep indentations at 2-N load.

| Experiment | Number of indentations | Initial load (N) | End load (N) | Indentation time (min) | Total time (min) |
|---|---|---|---|---|---|
| Short creep | 20 | 2.01 | 1.99 | 2 | 40 |
| Long creep | 4 | 2.10 | 1.90 | 20 | 80 |

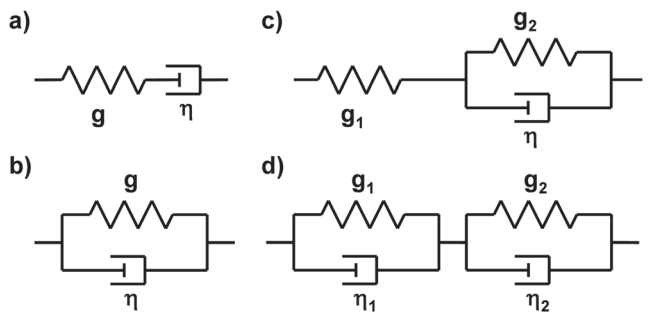


FIG. 3. Models composed by combinations of springs and dashpots: (a) Maxwell, (b) Voigt, (c) standard linear solid, and (d) double Voigt.

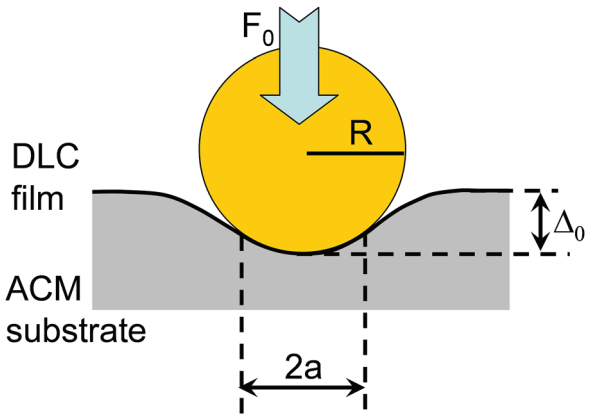


FIG. 4. (Color online) Scheme of the deformation of the rubber under spherical indentation assuming a Hertzian contact.

replacing the constant $1/(2G)$ by the creep compliance ($\phi$) of our particular viscoelastic arrangement. Thus, expression (2) can be re-written as:

$$\Delta_0 = \left(\frac{3}{8}R^{-1/2}F_0\phi\right)^{2/3}. \tag{3}$$

The creep compliance specifies the strain response to changes in stress. In the case of a SLS and a step change in stress, the creep compliance can be expressed as:

$$\phi = \phi_1 + \phi_2 = \frac{1}{g_1} + \frac{1}{g_2}\left(1 - \exp\left(-\frac{t}{T_2}\right)\right). \tag{4}$$

This system will show first an elastic deformation immediately after the application of the load $F_0$, whose magnitude is controlled by $g_1$. Then, it will deform with time depending on $T_2$, until reaching a maximum viscoelastic deformation controlled by $g_2$. Considering a sinusoidal evolution of the load (instead of a step change), expressions for the storage and loss modulus of the system depending on the spring and dashpots characteristics can be derived.[9]

Combining Eqs. (3) and (4), one obtains:

$$\Delta_0(t) = \left\{\frac{3}{8}R^{-1/2}F_0\left[\frac{1}{g_1} + \frac{1}{g_2}\left(1 - \exp\left(-\frac{t}{T_2}\right)\right)\right]\right\}^{2/3}. \tag{5}$$

However, the fitting procedure of the experimental data (Fig. 2) with this equation failed. We anticipated that the elastic deformation may be not immediate, but only much faster than the viscoelastic one. Therefore, the SLS model was modified by the addition of a second dashpot in parallel to the first spring, and thus leading to a double Voigt model (cf. Fig. 3(d)). The indentation depth according to this model can be written as:

$$\Delta_0(t) = \left\{\frac{3}{8}R^{-1/2}F_0\left[\frac{1}{g_1}\left(1 - \exp\left(-\frac{t}{T_1}\right)\right) + \frac{1}{g_2}\left(1 - \exp\left(-\frac{t}{T_2}\right)\right)\right]\right\}^{2/3}, \tag{6}$$

where $T_1$ should be much shorter than $T_2$ for a faster reaction of the first element. The fitting of the first cycle was successful, but further modification was needed to include the residual deformation accumulated in the rubber prior to the next indentations. When the rubber is unloaded, a certain recovery is obtained (see Fig. 5). Thus, the new cycle starts from a situation where a certain deformation is already produced, i.e., with an offset in the time:

$$\Delta_0(t) = \left\{\frac{3}{8}R^{-1/2}F_0\left[\frac{1}{g_1}\left(1 - \exp\left(-\frac{t + t_{01}}{T_1}\right)\right) + \frac{1}{g_2}\left(1 - \exp\left(-\frac{t + t_{02}}{T_2}\right)\right)\right]\right\}^{2/3}, \tag{7}$$

where $t_{0i}$, with $i = 1, 2$, are the offsets for both Voigt units (the fast and the slow one). As shown in Fig. 5, those times are not directly related to the loading and unloading times, because they account for the present deformation in the Voigt elements when the next loading cycle starts. In fact, the values of $t_{0i}$ typically increase with the number of cycles (see that $t_{0i}$ for the third cycle is larger than in the second one in Fig. 5). In addition, it has to be considered that the value of $t_{01}$ is different from the $t_{02}$, because the degree of deformation and recovery of both Voigt units is not the same during loading and unloading. Function 7 was used for fitting all of the curves from both experiments. In that procedure, the test conditions (load and ball radius) were known (the same as in the tribotests), and the material parameters ($g_1$, $g_2$, $T_1$, and $T_2$) were kept common and optimized together. The values of $t_{01}$ and $t_{02}$ were set as free parameters, except for the case of the first cycles of both experiments where they were set equal to zero. Figure 2 shows the fittings obtained for both sets of measurements described in Table I. The fittings show an excellent agreement with the experimental results in all of the measurements. The results obtained for ACM rubber at different loads are shown in Table II. It can be seen that the values obtained at lower loads are similar, whereas the values observed at 5 N are larger. This is particularly clear for the values of viscosity, which are a factor of four times larger than at 2 N. However, the $T_2/T_1$ and $g_2/g_1$ ratios are similar in all of the cases. Thus,

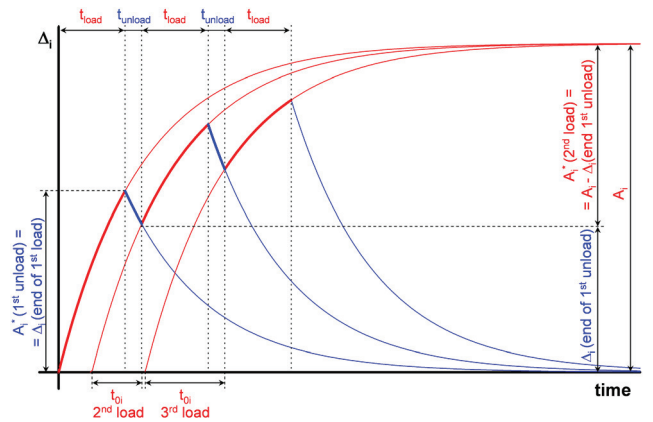


FIG. 5. (Color online) Deformation of a Voigt unit under loading and unloading cycles. The values of $A_i$* used for loading and unloading cycles during the simulation of depth variation in a tribotest are also depicted.

TABLE II. Mechanical properties of ACM rubber measured by creep experiments after fitting to a double Voigt model.

| | Indentation load (N) | | |
|---|---|---|---|
| Parameter | 1 | 2 | 5 |
| $g_1$ (GPa) | 0.35 | 0.46 | 0.63 |
| $g_2$ (GPa) | 0.25 | 0.28 | 0.39 |
| $\eta_1$ (GPa·s) | 2.5 | 3.9 | 14.7 |
| $\eta_2$ (GPa·s) | 20.5 | 23.7 | 85.2 |
| $T_1$ (s) | 7.2 | 8.5 | 23.5 |
| $T_2$ (s) | 81.9 | 85.1 | 218.0 |
| $g_2/g_1$ | 0.72 | 0.61 | 0.62 |
| $T_2/T_1$ | 11.4 | 10.0 | 9.3 |

in all of the cases, $T_2$ is around one order of magnitude larger than $T_1$, in agreement with two different kinetics of deformation. In addition, the ratio $g_2/g_1$ is lower than 1, indicating a larger maximum deformation of the slow Voigt unit.

### B. Simulation of the evolution of depth during a tribotest

The model used so far can be extended for simulating the indentation depth of a sliding ball at any position on a wear track when the ball consecutively passes it during a tribotest. For a wear track of radius $r$, the time for the ball to run a lap ($t_{\text{lap}}$) at sliding speed $V$ is:

$$t_{lap} = \frac{2\pi r}{V}. \tag{8}$$

The time of contact between the ball and one point is only a certain fraction of this time, and the unloading time (used for relaxation of the rubber) is the rest of the lap, as:

$$t_{load} \approx t_{lap}\frac{2a}{2\pi r}, \quad t_{unload} = t_{lap} - t_{load}, \tag{9}$$

where $a$ is the Hertzian radius of contact between the substrate and the ball, which can be calculated using Eq. (2):

$$t_{load} \approx \frac{2}{V}\left(\frac{3F_0R}{8}\left(\frac{1}{g_1}+\frac{1}{g_2}\right)\right)^{1/3}. \tag{10}$$

For tribotesting, Eq. (7) can be re-written as:

$$\Delta_0(t) = (\Delta_1+\Delta_2)^{2/3} = \left\{A_1 - A_1^*\exp\left(-\frac{t}{T_1}\right) + A_2 - A_2^*\exp\left(-\frac{t}{T_2}\right)\right\}^{2/3}. \tag{11}$$

$\Delta_i$ represent the temporal deformation of each Voigt element, with $i=1$ and $i=2$ for the "fast" and "slow" reacting Voigt units, respectively, and:

$$A_i = \frac{3}{8}\frac{R^{-1/2}F_0}{g_i}, \quad A_i^* = \frac{3}{8}\frac{R^{-1/2}F_0}{g_i}\exp\left(-\frac{t_{0i}}{T_i}\right). \tag{12}$$

Thus, $A_1$ and $A_2$ define the deformation of the double Voigt system at infinite time:

$$\Delta_0(t\to\infty) = (A_1+A_2)^{2/3}. \tag{13}$$

In the case of unloading, Eq. (11) needs to be modified as:

$$\Delta_0(t) = (\Delta_1+\Delta_2)^{2/3} = \left\{A_1^*\exp\left(-\frac{t}{T_1}\right) + A_2^*\exp\left(-\frac{t}{T_2}\right)\right\}^{2/3}, \tag{14}$$

because the deformation during unloading (ball passes away) is in the opposite direction (recovery), and its value at infinite time must be zero (full recovery). Both parameters $A_i^*$ can be considered as pre-exponential factors that control the magnitude of deformation of each Voigt element (see Fig. 5). During the first loading cycle, $A_i^* = A_i$, because $t_{0i} = 0$ (i.e., there is no previous deformation). However, during the next cycles, the values of $A_i^*$ depend on the final deformation of each Voigt element at the end of the previous loading cycle (see Fig. 5). Thus:

$$A_i^*(\text{unload}) = \Delta_i(\text{end of previous load cycle}), \tag{15a}$$

$$A_i^*(\text{load}) = A_i - \Delta_i(\text{end of previous unload cycle}). \tag{15b}$$

The combination of Eqs. (10)–(15) allows simulating the depth variation during a tribotest, as can be seen in Fig. 6(a). The continuous lines represent the simulation for a tribotest carried out in the same conditions as Fig. 1. They symbolize the maximum and minimum depth achieved on each lap, i.e., immediately after and before each pass of the ball, respectively. It can be seen that a steady state is reached at a value that agrees well with experimental observations (cf. Fig. 1), although its kinetics are too fast. One possible explanation is an underestimation of the relaxation times during the creep at the creep measurements; in fact, a more progressive depth evolution can be seen on a simulation performed using the larger viscosities obtained in the measurement performed at 5 N (cf. Table II), what are represented by dashed lines in Fig. 6(a). Figure 6(b) represents the deformation of each Voigt unit during the tribotest for the former case. Different deformation kinetics are observed for both elements, caused by their different values of relaxation time. In fact, the behavior is very similar to the one expected for a SLS (immediate elastic response followed by the viscoelastic deformation), although in this case the elastic deformation is not immediate, but much faster than the viscoelastic one. Thus, the double Voigt model can be considered as a small modification of the SLS. In addition, it can be seen that the deformation of the "fast" unit is smaller than the "slow" one, in agreement with the $g_2/g_1$ ratio (cf. Table II). Moreover, it can be seen that "fast" unit shows a greater difference between the maximum and minimum deformation than the "slow" unit (it can be better appreciated once the steady state is reached). In fact, the "fast" unit is responsible for the difference observed in the overall system (cf. Fig. 6(a) in the steady state), an effect not observed in the simulation for larger values of $\eta_i$ (both dashed lines appear together). This is caused by the deformation sequence during the tribotest,

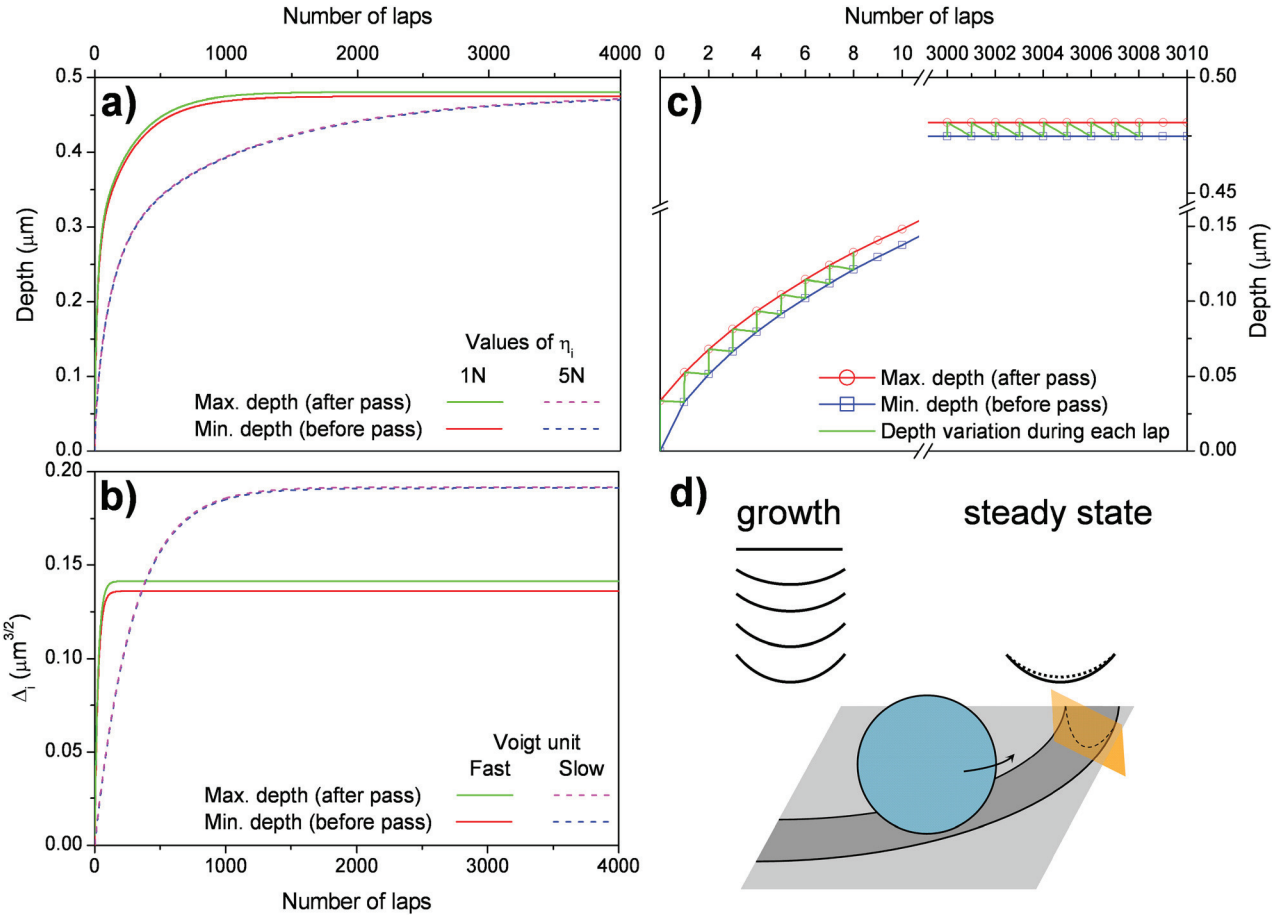


FIG. 6. (Color online) Results of the depth simulation during tribotest for ACM rubber using the same conditions as in Fig. 1. (a) Evolution of depth; for comparison purposes, the simulation using higher values of viscosity (cf. Table II) is also depicted with dashed lines. (b) Contribution of each Voigt element to the overall deformation. (c) Detailed view of the depth evolution during each cycle, at the beginning of the tribotest, and once the steady-state condition has been reached. (d) Sketch illustrating the evolution of the cross section of the tribotrack during both situations.

which is depicted in Figs. 6(c) and 6(d). Figure 6(c) shows a magnified view of two regions of Fig. 6(a) (the beginning of the test and the steady state), including the variation of deformation taking place during each lap. It can be seen that the loadings cause a deep increase of deformation in every lap, and this deformation is relaxed in the unloading period. At the beginning of the test, the relaxation is not enough to recover the deformation occurred during the loading, and the overall depth increases. This is sketched in Fig. 6(d) as a progressive increase of the cross section of the tribotrack during the test. In contrast, when the steady-state condition is reached, the deformation caused during the loading fraction of the lap is recovered during the unloading fraction. Therefore, the cross section is kept confined between the minimum and maximum values observed immediately before and after the loading, respectively. The magnitude of this variation depends mainly on the relaxation time of the "fast" Voigt unit ($T_1$), because a low value allows its rapid response to the (un)loading. Thus, in case of larger viscosities, the maximum and minimum depths are much closer (cf. Fig. 6(a), and the "slow" Voigt unit in Fig. 6(b)).

Although this model gives good values of depth achieved by the ball and provides a good qualitative explanation about rubber behavior during the tribotest, it has two major drawbacks. First, the deformation kinetics are not correct, which can be related to the underestimation of the viscous parameters during its measurement, or more probably caused by the rough approach used for the estimation of the contact time during each pass. In addition, a tribotest is not a sequence of indentations at a given frequency, but also the presence of lateral forces must be considered. As a consequence, this model cannot indicate anything about the behavior of the friction during the tribotest. Therefore, a different approach is needed for that kind of analysis, which is studied in another paper.[7]

## IV. CONCLUSIONS

The evolution of the ball depth on DLC film-coated ACM rubber during tribological tests has been analyzed using simple viscoelastic models. The viscoelastic parameters were estimated by a creep test using spherical indentation and fitting to a double-Voigt model. The depth increases in each pass of the ball over the rubber, and recovers in the interval of sliding. Thus, the overall depth increases at the beginning of the test until reaching a steady state. The kinetics and values of depth during the tribotest can be accurately simulated using the viscoelastic properties obtained experimentally.

## ACKNOWLEDGMENTS

This research was carried out under Project No. MC7.06247 in the framework of the Research Program of the Materials Innovation Institute M2i (www.m2i.nl), Delft, the Netherlands. Dr. X.B. Zhou of the SKF Engineering & Research Center in Nieuwegein, the Netherlands is thanked for his valuable input.

[1]M. Schenkel, D. Martinez-Martinez, Y. T. Pei, and J. T. M. De Hosson, Surf. Coat. Technol. **205**, 4838 (2011).
[2]D. Martinez-Martinez, M. Schenkel, Y. T. Pei, and J. T. M. De Hosson, Thin Solid Films **519**, 2213 (2011).
[3]D. Martinez-Martinez, M. Schenkel, Y. T. Pei, and J. T. M. De Hosson, Surf. Coat. Technol. **205**, S75 (2011).
[4]Y. T. Pei, X. L. Bui, and J. T. M. De Hosson, Scr. Mater. **63**, 649 (2010).
[5]X. L. Bui, Y. T. Pei, E. D. G. Mulder, and J. T. M. De Hosson, Surf. Coat. Technol. **203**, 1964 (2009).
[6]J. Robertson, Mater. Sci. Eng. R **37**, 129 (2002).
[7]D. Martinez-Martinez, J. P. van der Pal, Y. T. Pei, and J. T. M. De Hosson, J. Appl. Phys. (submitted).
[8]X. L. Bui, Y. T. Pei, E. D. G. Mulder, and J. T. M. De Hosson, in *Surface Effects and Contact Mechanics IX—Computational Methods and Experiments, Algarve, Portugal, June 2009*, edited by J. T. M. De Hosson and C.A. Brebbia (WIT Press), p. 73.
[9]D. F. Moore, *The Friction and Lubrication of Elastomers* (Pergamon, New York, 1972).
[10]K. L. Johnson, *Contact Mechanics* (Cambridge University Press, Cambridge, 1987).
[11]J. R. M. Radok, Q. Appl. Math. **15**, 198 (1957).